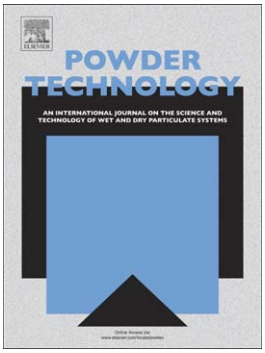

CFD-DEM investigation of particle elutriation with electrostatic effects in gas-solid fluidized beds

Yao Yang, Can Zi, Zhengliang Huang, Jingdai Wang, Musango Lungu, Zuwei Liao, Yongrong Yang, Hongye Su

PII: S0032-5910(16)30900-7
DOI: doi:10.1016/j.powtec.2016.12.032
Reference: PTEC 12180

To appear in: *Powder Technology*

Received date: 10 August 2016
Revised date: 5 December 2016
Accepted date: 8 December 2016

Please cite this article as: Yao Yang, Can Zi, Zhengliang Huang, Jingdai Wang, Musango Lungu, Zuwei Liao, Yongrong Yang, Hongye Su, CFD-DEM investigation of particle elutriation with electrostatic effects in gas-solid fluidized beds, *Powder Technology* (2016), doi:10.1016/j.powtec.2016.12.032

CFD-DEM investigation of particle elutriation with electrostatic effects in gas-solid fluidized beds

Yao Yang [a], Can Zi [a], Zhengliang Huang *[a], Jingdai Wang [a], Musango Lungu [a], Zuwei Liao [a], Yongrong Yang [a] and Hongye Su [b]

[a] State Key Laboratory of Chemical Engineering, College of Chemical and Biological Engineering, Zhejiang University, Hangzhou, 310027, China

[b] College of Control Science and Engineering, Zhejiang University, Hangzhou, 310027, China

*Correspondence to the author, e-mail: huangzhengl@zju.edu.cn

Abstract: Unsuccessful prediction of particle elutriation in fluidized beds is in part due to the negligence of electrostatic effects. In addition, lack of properly designed experiments makes it difficult to quantify the effects of electrostatics on particle elutriation. In this work, the CFD-DEM modeling approach has been used for the first time to investigate particle elutriation in a 2D fluidized bed taking into account electrostatic effects. Model predictions show that electrostatic charges on particles suppress particle elutriation and even eliminate elutriation completely at relatively higher charge levels. The study further shows that electrostatic effects result in the increase of the fluidized bed height and axial velocity of small particles in free board which ultimately promotes particle elutriation. However, the presence of agglomerates caused by electrostatic attractions is dominant, thus the decrease in the concentration of small particles in the free board suppresses particle elutriation.

Key words: fluidized bed; electrostatic effects; particle elutriation; CFD-DEM modeling

1. Introduction

In gas-solid fluidized beds, fine particles whose terminal velocities are smaller than the superficial gas velocity, are splashed into the free board at the bed surface and eventually transported out of the fluidized bed, this is known as particle elutriation [1]. Particle elutriation is common and a major disadvantage of gas-solid fluidized bed reactors [2]. An in-depth understanding of this phenomenon is one of the preconditions for successful design of particles separators and recovery equipment, and is also the key to successful and economic applications of gas-solid fluidized bed reactors [2-4]. Several correlations [5-11] exist from the open literature for predicting elutriation rates of fine particles based on experimental results or hydrodynamic principles, however predicted elutriation rates using these

correlations differ from each other by several orders of magnitude [3, 12]. One of main reasons for the difference in predictions is the negligence of electrostatic effects on particle elutriation [2, 3]. In fluidized beds, electrostatic charges can be generated and accumulated on account of repeated particle-particle and particle-wall collisions and frictions [13]. Extra accumulation of electrostatic charges will change the resultant forces on particles [14, 15] which then alters the hydrodynamic behaviors in the bed [16] including particle elutriation. Therefore, the experimental system with the consideration of electrostatic effects is essential for the deviation of correlations in order to obtain meaningful results [10, 17].

Reduction of particle elutriation under the action of static electricity in gas-solid fluidized beds is first reported by Baron et al. [18], and this phenomenon was further reinforced by investigations of Briens et al. [19] and Li et al. [20]. However, these studies only established a simple relationship between electrostatic phenomena and particle elutriation, detailed studies on the influence of electrostatic forces on particle elutriation are still rather scarce. On the other hand, in researching the particle elutriation of fluidized bed, the electrostatic charges in fluidized beds are always eliminated by increasing the humidity of fluidizing air [21]. Nevertheless, the particles are fluidized in relatively dry environment in most industrial processes, which is conducive for the generation and accumulation of electrostatic charges. As a consequence, the research results by ignoring the electrostatic effects could not be used for the comprehensive understanding of particle elutriation in industrial processes. From the above analysis, it is of vital importance to investigate the particle elutriation with electrostatic effects in gas-solid fluidized beds.

Currently, particle elutriation is mainly investigated using experimental tools. Particle elutriation rates are acquired by sampling and weighting [21], electrostatic impact probes [22], optical probes [23] and mass flux probes [18]. Besides, with the rapid development of multi-fluid computational fluid dynamic (CFD) modeling in recent years[24-27], the particle elutriation can also be investigate by CFD simulation [28]. However, the drawbacks of the aforementioned methods are apparent. The sampling and weighting method does not give any information about the concentrations and velocities of fine particles in the free board. Although methods using probes detect concentrations and velocities of fine particles in the free board, particle clustering effects interfere with the results [4]. What's worse, controlling the electrostatic levels quantitatively by experimental methods is very different. Euler-Euler

CFD models treat both the gas and solid phase as interpenetrating continuums, thus the dynamic behaviors of individual particles cannot be reflected directly. Therefore, finding a more accurate method to study the principle of particle elutriation as well as electrostatic effects is of utmost importance. In recent years, the CFD-DEM approach, a Eulerian-Lagrangian modeling category which combines the computational fluid dynamics (CFD) and discrete element method (DEM), has been widely applied as an effective approach to study the fundamentals of the gas-solid fluidization [29-32]. Furthermore, because the electrostatic charges on particles can be set quantitatively by CFD-DEM modelling, this method has demonstrated its potential and advantages in studying electrostatic effects in gas-solid fluidized beds. Using this method, Lim et al. [33] studied the electrostatic effects on the mixing behaviors in a fluidized bed. Hassani et al. [34] investigated the effects of electrostatic forces on the hydrodynamics of gas-solid fluidized beds. Therefore, the CFD-DEM model is an effective method to investigate the particle elutriation and even effects of electrostatics on particle elutriations in the particle level.

In this work, the CFD-DEM modeling is applied for the first time in the study of particle elutriation in a gas-solid fluidized bed. The model was first validated against empirical data and thereafter used to investigate the electrostatic effects on particle elutriation. The effect mechanism was also revealed by analyzing the height of the fluidized bed, the concentration and vertical velocity distribution of fine particles in the free space, and the agglomeration caused by electrostatic forces.

2. Computational models

The CFD-DEM modeling approach has been previously reviewed by other researchers [29, 32], therefore, for the sake of brevity only a brief description of the equations used in this work is given.

2.1 Governing equations of solid phase

In this work, the solid phase consists of discrete particles, and the motion for each particle is described by Newton's second law. The translational and rotational motions of a specific particle i with the mass of m_i can be formulated as:

$$m_i \frac{d\mathbf{v}_i}{dt} = m_i\mathbf{g} + \mathbf{f}_{\mathbf{p},i} + \mathbf{f}_{\mathbf{d},i} + \sum_{j=1}^{N_j}\mathbf{f}_{\mathbf{c},ij} + \sum_{k=1}^{N_k}\mathbf{f}_{\mathbf{e},ik} \quad (1)$$

$$I_i \frac{d\boldsymbol{\omega}_i}{dt} = \sum_{j=1}^{N_c}(\mathbf{M}_{\mathbf{t},ij} + \mathbf{M}_{\mathbf{r},ij}) \quad (2)$$

where $\mathbf{v}_i$、$\boldsymbol{\omega}_i$ and I_i are, respectively, the translational velocities, the rotational velocities and the

moment of inertia of particle *i*. From Eq. (1), forces on particle *i* include the gravity $m_i\mathbf{g}$, the drag force $\mathbf{f}_{\mathbf{d},i}$, the contact force $\mathbf{f}_{\mathbf{c},ij}$, the inter-particle electrostatic force $\mathbf{f}_{\mathbf{e},ik}$ and the far field pressure gradient force $\mathbf{f}_{\mathbf{p},i}$.

Numerous models have been published to calculate the drag forces on particles in gas-solid systems. Considering the fact that in the fluidized bed there exist both high voidage region (in the free board) and low voidage region (in the dense bed), a model that combines the Ergun equation and the correlation proposed by Wen and Yu was used in this work [3]. Calculation of contact forces on particles significantly affects the calculation time. Previous investigations demonstrated that the calculation time could be reduced by using the linear-spring and dashpot model proposed by Cundall and Strack, meanwhile the accuracy of the simulation results could be maintained [3]. In consequence, the linear-spring and dashpot model was used in this work. Particle-particle electrostatic forces were calculated based on the screened Coulomb's law [35], and the screening radius with a value of 5 times the particle radius was used. A summary of the modeling details are shown in Table 1.

Table 1. Equations of forces and torque acting on particle *i*

Symbol	Forces and torque		Equations
$\mathbf{f}_{\mathbf{d},i}$	Drag force		$\mathbf{f}_{\mathbf{d},i}=\frac{V_i\beta}{\varepsilon_s}(\mathbf{u}-\mathbf{v}_i)$, $\beta=\begin{cases}150\frac{\varepsilon_s^2}{\varepsilon_g}++1.75\varepsilon_s Re_i & \text{if } \varepsilon_g<0.8,\\ \frac{3}{4}C_D Re_i\ \varepsilon_s\varepsilon_g^{-2.65} & \text{if } \varepsilon_g\geq 0.8,\end{cases}$ $C_D=\begin{cases}24(1+0.15Re_i^{0.687})/Re_i & \text{if } Re_i<10^3,\\ 0.44 & \text{if } Re_i\geq 10^3,\end{cases}$ where: $Re_i=\varepsilon_g\rho_g\left\|\mathbf{u}-\mathbf{v}_i\right\|d_{p,i}/\mu_g$, $\varepsilon_g+\varepsilon_s=1$
$\mathbf{f}_{\mathbf{c},ij}$	Contact forces	Normal	$\mathbf{f}^n_{\mathbf{c},ij}=-(k_n\delta_{n,i})\mathbf{n}_{ij}-(\eta_{n,i}\mathbf{v}_{n,ij}\mathbf{n}_{ij})\mathbf{n}_{ij}$ where: $\mathbf{R}_i=\mathbf{r}_j-\mathbf{r}_i, \mathbf{n}_{ij}=\mathbf{R}_i/\left\|\mathbf{R}_i\right\|, \mathbf{v}_{n,ij}=\mathbf{v}_i-\mathbf{v}_j$
		Tangential	$\mathbf{f}^t_{\mathbf{c},ij}=\begin{cases}-(k_t\delta_{t,i})\mathbf{t}_{\mathbf{ij}}-(\eta_{t,i}\mathbf{v}_{t,ij}\mathbf{t}_{\mathbf{ij}})\mathbf{t}_{\mathbf{ij}} & \text{if } \left\|\mathbf{f}^t_{\mathbf{c},ij}\right\|\leq\mu_f\left\|\mathbf{f}^n_{\mathbf{c},ij}\right\|,\\ \mu_f\left\|\mathbf{f}^n_{\mathbf{c},ij}\right\|\mathbf{t}_{\mathbf{ij}} & \text{if } \left\|\mathbf{f}^t_{\mathbf{c},ij}\right\|>\mu_f\left\|\mathbf{f}^n_{\mathbf{c},ij}\right\|,\end{cases}$ where: $\mathbf{v}_{t,ij}=\mathbf{v}_{n,ij}\cdot\mathbf{t}_{\mathbf{ij}}+(\boldsymbol{\omega}_i\times\mathbf{R}_i-\boldsymbol{\omega}_i\times\mathbf{R}_j)$
$\mathbf{f}_{\mathbf{e},ik}$	Electrostatic force		$\mathbf{f}_{\mathbf{e},ik}=\frac{q_iq_k}{4\pi\varepsilon_0}\left(\frac{\kappa}{\left\|\mathbf{r}_i-\mathbf{r}_k\right\|}+\frac{1}{\left\|\mathbf{r}_i-\mathbf{r}_k\right\|^2}\right)e^{-\kappa\left\|\mathbf{r}_i-\mathbf{r}_k\right\|}(\mathbf{r}_i-\mathbf{r}_k)$

where: $\kappa = q_e\sqrt{\left(\frac{1}{\varepsilon\varepsilon_0 K_B T}\sum_i n_i z_i^2\right)}$

$\mathbf{f}_{\mathbf{p},i}$	Pressure gradient force	$\mathbf{f}_{\mathbf{p},i} = -V_i\nabla p$
$\mathbf{T}_i$	Torque	$\mathbf{T}_i = \mathbf{R}_i \times \mathbf{f}^t_{\mathbf{c},ij} - \mu_r R_i \left\|\mathbf{f}^n_{\mathbf{c},ij}\right\| \hat{\omega}_{ij}$ where: $\hat{\omega}_{ij} = \frac{\omega_i - \omega_j}{\left\|\omega_i - \omega_j\right\|}$

2.2 Governing equations of gas phase

The motion of the gas phase is described by the continuity equation and Navier–Stokes equations formulated as follows:

$$\frac{\partial(\rho_g \varepsilon_g)}{\partial t} + \nabla\bullet\left(\rho_g \varepsilon_g \mathbf{u}\right) = 0 \quad (3)$$

$$\frac{\partial(\rho_g \varepsilon_g \mathbf{u})}{\partial t} + \nabla\bullet\left(\rho_g \varepsilon_g \mathbf{u}\mathbf{u}\right) = -\varepsilon_g \nabla P + \nabla\bullet\left(\varepsilon_g((\lambda_g - \frac{2}{3}\mu_g)(\nabla\bullet\mathbf{u})\mathrm{I} + \mu_g(\nabla\mathbf{u} + \nabla\mathbf{u}^T))\right) + \rho_g \varepsilon_g \mathbf{g} + \mathbf{S}_{s\to g} \quad (4)$$

where ρ_g, ε_g, P and $\mathbf{u}$ are the density of fluidizing gas, the average voidage of the computational cell, the pressure, and the velocity vector of gas respectively. The last item in the right-hand side of the Eq. (4) is the total fluid-particle interaction source expressed as:

$$\mathbf{S}_{s\to g} = -\sum_{i=1}^{N_i}(\mathbf{f}_{\mathbf{d},i} + \mathbf{f}_{\mathbf{p},i})/V_c \quad (5)$$

where V_c is the volume of the present computational cell.

The flow regime in the bed is classified as turbulent fluidization (details shown in Section 4.1) based on the superficial velocities employed. Therefore, the gas viscosity μ_g shown in Eq. (4) is the dynamic viscosity of the gas phase, and is the sum of the fluid molecular viscosity $\mu_{g,\,\text{laminar}}$ and the turbulent viscosity $\mu_{g,\,\text{turbulent}}$. The turbulent viscosity is computed from Eq. (6).

$$\mu_{g,\text{turbulence}} = c_\mu \rho_g k^2/\varepsilon_t \quad (6)$$

where k and ε_t are the turbulent kinetic energy and dissipation rate respectively. They are govern by Eq. (7) and (8) respectively.

$$\frac{\partial \rho_g \varepsilon_g k}{\partial t} + \nabla\bullet\left(\rho_g \varepsilon_g \mathbf{u} k\right) = \nabla\bullet\left(\varepsilon_g(\mu_{g,\,\text{laminar}} + \frac{\mu_{g,\,\text{turbulent}}}{\sigma_k})\nabla k\right) + \varepsilon_g G_k - C_D \rho_g \varepsilon_g \varepsilon \quad (7)$$

$$\frac{\partial \rho_g \varepsilon_g \varepsilon_t}{\partial t} + \nabla\bullet\left(\rho_g \varepsilon_g \mathbf{u} \varepsilon_t\right) = \nabla\bullet\left(\varepsilon_g(\mu_{g,\,\text{laminar}} + \frac{\mu_{g,\,\text{turbulent}}}{\sigma_k})\nabla \varepsilon_t\right) + \frac{\varepsilon_g \varepsilon_t}{k}(C_1 G_k - C_2 \rho_g \varepsilon_t) \quad (8)$$

where: $G_k = \mu_{g,\,\text{turbulent}}\left(\frac{\partial u_i}{\partial x_j} + \frac{\partial u_j}{\partial x_i}\right)\frac{\partial u_i}{\partial x_j}$

In Eq. (6), (7) and (8), the values of constants used are [36, 37]: C_μ=0.09, C_D=1.00, C_1=1.44,

C_2=1.92, σ_k=1.00, σ_ε=1.30.

3. Simulation conditions

The computational domain is a rectangular two-dimensional fluidized bed, 70×6×1200 mm shown in Figure 1. The simulation was initialized by randomly generating 31620 large polyethylene (PE) particles with the diameter of 1 mm and 13315 small PE particles with the diameter of 0.5 mm in the domain at velocities of 63240 s^{-1} and 26630 s^{-1} separately. The particles fall under the action of gravity and form a packed bed with a static height of 110 mm.

Triboelectric charging of insulated particles is a relative complex process. In this process, the amount of charge on particles increases exponentially with contact time, and finally reaches a saturated value when the generation rate equals to the dissipation rate [38-40]. This work is aimed at studying particle elutriation at various saturated electrostatic charges, which means that the generation and dissipation mechanisms are not considered. Namely, the amount of charge on particles is set to a certain value at the beginning of each simulation and kept constant during the whole simulation. This method was also used by other researchers [33, 34] successfully. Fang et al. [41] proposed that larger PE particles had a tendency to be negatively charged while smaller particles always had a tendency to be charged positively in a 3D gas-solid fluidized bed. In the current work, particles with a diameter of 1 mm were set to be charged negatively, while particles with a diameter of 0.5 mm were charged positively. According to Gauss's law, for a particle surrounded by dried air, the maximum amount of charge on it can be calculated as follow [14].

$$|q|_{\max} = 2.64\times10^{-5}(\pi d_p^2)(\frac{3\varepsilon_r}{2+\varepsilon_r}) \quad (9)$$

where ε_r is the relative permittivity of particles.

From Eq. (9), the maximum amount of charge $|q|_{\max}$ carried by large and small particles used in this work are 0.133 and 0.033 nC separately. In a two dimensional domain, the particle-wall electrostatic forces are not considered, which means that triboelectric charging only exists between different kinds of particles and the total charge carried by all particles should be zero. Based on this, it is assumed firstly that amount of charge carried by large particles reached the maximum value during the tribocharing process, namely -0.133 nC. Then amount of charge on small particles will be calculated and it is +0.316 nC. Obviously, it is larger than the theoretical maximum amount of charge on small particles (0.033 nC). Therefore, the above assumption is wrong and which means that amount of charge on small

particle will reach the maximum value (+0.033 nC) during the tribocharing process. Then the $|q|_{max}$ is calculated and it is -0.014 nC/+0.033 nC for large and small particles separately. In consequence, the amount of charge on particles q_p was set to three different cases: -0.014 nC/+0.033 nC，-0.007 nC/+0.017 nC，-0.003 nC/+0.008 nC. Obviously these three cases corresponded to three different levels of charge, specifically, 25%, 50% and 100% of the $|q|_{max}$. Other details about simulation conditions can be found in Table 2.

Table 2. Details of simulation conditions

Geometry		
Dimensions (mm)	70 length ×6 width × 1200 height	
Computational grids (mm)	2 length ×2 width ×2 height	
Particles		
Materials	Polyethylene	
Density (kg/m^3)	918	
Numbers	Big particles: 31620	Small particles: 13315
Diameter (mm)	Big particles: 1	Small particles: 0.5
Geldart's classification	Big particles: Geldart B group	small particles: Geldart B group
Minimum fluidization velocity (m/s)	Big particles: 0.24	Small particles: 0.07
Terminal velocity (m/s)	Big particles: 4.81	Small particles: 2.01
Charges (nC)	Big particles: - 0.014, - 0.007,- 0.003	Small particles: 0.033, 0.017, 0.008
Restitution coefficient	Inter-particle: 0.8	Particle-wall: 0.8
Friction coefficient	Inter-particle: 0.3	Particle-wall: 0.3
Gas phase		
Materials	Air	
Density (kg/m^3)	1.225	
Viscosity (Pa s)	1.81×10^{-5}	
Superficial gas velocity (m/s)	2.2, 2.3, 2.4, 2.5	

In the simulation, inlet and outlet boundary conditions were set as velocity-inlet and outflow, respectively. The gas entered the bed uniformly at the bottom of column. In order to eliminate the influences of the back and front walls on the gas flow, the boundary conditions of the front and back walls were set as symmetry. Different discretization methods were used for different variables, for volume fraction, QUICK scheme was adopted, while for other terms, second-order upwind discretization scheme was used. The time steps for DEM and CFD were 1×10^{-6} s and 2×10^{-5} s respectively. The real time of 5 s was calculated for each simulation.

4. Results and discussions

4.1 Model verification

4.1.1 Flow regime and pressure drop

Firstly the simulation was conducted without electrostatic effects at four different superficial gas velocities, i.e. 2.2, 2.3, 2.4, and 2.5 m/s. Then the simulated flow regimes and pressure drops of the entire bed were analyzed to validate the accuracy of the simulated model. Horio [42] developed a correlation for the transition velocity from the bubbling fluidization to turbulent fluidization u_c, which could be used in a wide range of particle size (0.54-2.6 mm). The correlation is shown as follow.

$$u_c = \frac{0.936 Ar^{0.472} \mu_g}{\bar{d}_p \rho_p} \quad (10)$$

where $\bar{d}_p$ is the average diameter of particles, and Ar is the Archimedes number, which can be expressed as Eq. (11).

$$Ar = \bar{d}_p^3 \rho_p (\rho_p - \rho_g) g / \mu_g^2 \quad (11)$$

By Eq. (10), the transition velocity is 1.93 m/s for the particles used in this work. As a result, all the simulated flow regimes should be in the condition of turbulent fluidization.

Figure 2 is the instantaneous snapshots (t = 4 s) of the simulated fluidized bed at the superficial gas velocity of 2.2 m/s. Figure 2 shows that there are no bubbles in the bed, and the gas mainly exists as voids. Therefore, a preliminary judgment that the flow regime in the simulated bed is in turbulent fluidization regime can be made. Moreover, Figure 3 and 4 show the pressure fluctuations of the entire bed and the standard deviations of the pressure fluctuation at different superficial gas velocities respectively. Comparing the pressure fluctuation signals shown in Figure 3 with signals in a turbulent bed measured by Bi at al. [43], it can be found that they fluctuate with the same trend, namely, signals fluctuate up and down around an average value, but the amplitudes of the upward fluctuations are always larger. From Figure 4, the standard deviation of pressure fluctuation decreases as the superficial gas velocity increases. According to the investigation of van Ommen et al. [44], the standard deviation of pressure fluctuation can be used to judge the transition of flow regime in fluidized beds. At the transition velocity, the standard deviation of pressure fluctuation is the largest, and as the flow regime is changed into the turbulent fluidization, the standard deviation of pressure fluctuation decreases with

the increase of superficial gas velocity. So this result reinforces that the simulated flow regime is turbulent fluidization. Besides, the simulated pressure drops of the entire bed at different superficial gas velocities are also compared with the static pressure drop calculated by the weight of the entire bed in Figure 4. The result shows that the simulated pressure drops are close to the static pressure drop, but the former is always larger than the latter. This might be caused by extra frictions between the particles and the front/back walls [45]. Totally, the results shown above all exhibit that accurate flow regimes and pressure drops are acquired by this model.

4.1.2 The elutriation rate

In general, the elutriation rate is formulated as Eq. (12), just the same with the equation for the reaction rate of the first-order reaction.

$$-\frac{\mathrm{d}X_i}{\mathrm{d}t} = KX_i \quad (12)$$

where X_i is the mass fraction of specific particles, and K is the elutriation rate constant. By solving Eq. (12), the mass fraction of the specific particles changes exponentially with time, and it can be expressed as follow.

$$X_i = X_{i0}\exp(-Kt) \quad (13)$$

But it is clear that the elutriation rate constant K in Eq. (12) and (13) cannot represent the variation of the particles amount. In addition, Yagi et al. [5] developed another way to represent the elutriation rate, which can be formulated as Eq. (14).

$$\frac{\mathrm{d}(WX_i)}{A\mathrm{d}t} = -E_{i\infty}X_i \quad (14)$$

where W is the total mass of the specific particles, A is the cross-sectional area of the fluidized bed and $E_{i\infty}$ is the elutriation rate which shows changes in the mass of particles. Comparing Eq. (12) with (14), the relationship between the elutriation rate constant K and the elutriation rate $E_{i\infty}$ can be expressed as Eq. (15).

$$E_{i\infty} = \frac{KW}{A} \quad (15)$$

Therefore, the elutriation rate constant of small particles is acquired by calculating variation of mass fraction of small particles with time and then the elutriation rate of small particles is further calculated by Eq. (15).Taking the case at the superficial gas velocity of 2.2 m/s as an example, Figure 5 shows the variation of mass fraction of small particles with time and the fitting result of the elutriation rate

constant. According to Figure 5, the simulated elutriation rate at 2.2 m/s was calculated and which was 0.46 kg/m^2·s.

Wen et al. [10] reviewed a lot of elutriation correlations and found that a correlation developed by an experimental system similar to the one being predicted is essential to acquire an accurate prediction. Comparing the simulation conditions in this work with other researchers' experimental conditions, the simulation conditions in this work are covered by Tanaka's experimental conditions [9]. As a result, the correlation raised by Tanaka was used to validate the simulated elutriation rate, and is given as:

$$\frac{E_{i\infty}}{\rho_g(u_0-u_t)} = 0.045\left[\frac{(u_0-u_t)^2}{gd_p}\right]^{1/2} Re_t^{0.3}\left(\frac{\rho_p-\rho_g}{\rho_g}\right) \quad (16)$$

where u_0 and u_t are the superficial gas velocity and the terminal velocity of small particles, and Re_t is Reynolds number of small particles at the terminal velocity, which can be expressed as Eq. (17).

$$Re_t = d_p u_t \rho_g / \mu \quad (17)$$

In Table 3, the simulated elutriation rates at different superficial gas velocities are compared with the empirical values calculated from Eq. (16). According to Table 3, the simulated elutriation rate increases with the superficial gas velocity, which shares the same trend with the the empirical correlation. A closer inspection of the simulated results reveals that the simulated elutriation rate is always larger than the empirical value at any given gas velocity. The reason for this deviation is that the empirical values are the saturated elutriation rates beyond the transport disengagement height (TDH), while in this work the height of the free board might be smaller than the TDH and then leads to an over estimation of the elutriation rate. Besides, the electrostatic charges in the experiments performed by Tanaka et al. has not been eliminated. Considering the fact that electrostatic charges in fluidized bed reduce the particle elutriation [18-20], it seems reasonable that the simulated results are greater than the results calculated by Tanaka et al.'s correlation. In summary, for superficial gas velocities larger than 2.3 m/s, the relative error between the simulated results and the empirical values is consistently lower than 20%. It can be safely concluded that particle elutriation is well predicted using this model.

Table 3. Comparisons between the simulated elutriation rates and the empirical elutriation rates at different superficial gas velocities

Superficial gas velocity (m/s)	Simulated results ($kg/m^2 \cdot s$)	Calculated by Tanaka's correlation ($kg/m^2 \cdot s$)	Relative error (-)
2.2	0.46	0.34	0.35
2.3	0.91	0.73	0.25
2.4	1.49	1.27	0.17
2.5	2.29	1.96	0.17

4.2 Electrostatic effects on particle elutriation

After the validation exercise, the model was further used to investigate electrostatic effects on particle elutriation. From Section 4.1, the relative errors between the simulated elutriation rates and the empirical values were much smaller at high superficial gas velocities, so the superficial gas velocity was chosen as 2.4 m/s for the investigations of particle elutriation with electrostatic effects.

Figure 6 compares the variation of mass fraction of small particles from 1 to 5 s for different levels of charge. From Figure 6, when particles are uncharged, mass fraction of small particles in the bed decreases exponentially with time, and according to the method developed in Section 4.1.2, the elutriation rate can be calculated as 1.49 $kg/m^2 \cdot s$. When q_p is increased to 25% of the $|q|_{max}$, mass fraction of small particles also decreases exponentially with time, but the mass fraction of small particles in this case is always greater than the uncharged case and the calculated elutriation rate is 1.41 $kg/m^2 \cdot s$. In consequence, electrostatic charges on particles are considered as the reason for the decrease of elutriation rate, which is in good agreement with other researchers' results [18, 20, 28]. Further increase of q_p to 50% and 100% of the $|q|_{max}$, electrostatic charges on particles affects the mass fraction of small particles in the bed obviously and the particle elutriation disappears.

4.3 Effect mechanism of electrostatic charges on particle elutriation

In section 4.2, the modeling results show that electrostatic charges on particles brings about the decrease of elutriation rate, but the fundamental working mechanism is still unclear. Generally speaking, elutriation is a process in which small particles are separated from the fluidized bed at the bed surface, transported through the free board and finally out of the fluidized bed reactor. Therefore, it is affected by the physical properties of small particles, the hydrodynamic behaviors of the fluidized bed as well as the dynamic behaviors of small particles in the free board. In the subsequent sections, electrostatic effects on the height of the fluidized beds, the concentration and axial velocity distribution

of fine particles in free board, and the agglomerations will be analyzed. Finally the fundamental working mechanism will be discussed.

4.3.1 Height of the fluidized bed

In this work, the average particle height $<h_p>$ was used to represent the height of the fluidized bed, which has been used by Goldschmidt et al. [46] to study the bed expansion dynamics in their investigation. In details, the simulated fluidized bed in this work was divided into 40 layers, then the height of each layer was 30 mm and the center of layer i was (15+30×(i-1)) mm in height. Assuming that particles in the layer i were all equal to the center of this layer in height, the average particle height can be calculated as:

$$\left\langle h_p \right\rangle = \frac{\sum_{k}^{N_p} h_k}{N_p} = \frac{\sum_{i=1}^{40} \varepsilon_{s,i} h_i}{\sum_{i=1}^{40} \varepsilon_{s,i}} = \frac{\sum_{i=1}^{40} (15+30\times(i-1))\varepsilon_{s,i}}{\sum_{i=1}^{40} \varepsilon_{s,i}} \quad (18)$$

where $\varepsilon_{s,i}$ is the particle concentration in layer i.

Four different cases in which the charge level is 0%, 25%, 50% and 100% of the $|q|_{max}$ separately are simulated and the average heights of different kinds of particles in these four cases are compared in Figure 7. From Figure 7-a, at any level of charge the fluidized bed has reached a steady state at 2 s and after that the average height of all particles always fluctuates around a stable value over time, although this stable height at different levels of charge is different. To be specific, the stable height increases with q_p, as q_p is lower than 50% of the $|q|_{max}$. While as q_p further increases to 100% of the $|q|_{max}$, the stable height decreases slightly instead of increasing. In the modeling set up, most of the negatively charged particles are large particles, and the electrostatic repulsive forces among these particles make the average height of all particles increase in a certain range. The result in the work of Hassani et al. [34] is consistent with this result, by CFD-DEM modeling, they found that in a fluidized bed filled with mono-charged particles, the particle-particle electrostatic repulsive forces made the voidage of the emulsion phase increased. However, as q_p becomes large enough, the electrostatic attractions between negatively and positively particles would promote the formation of agglomerates. Furthermore, the agglomerates might lead to channeling and then lead to the decrease of the average height of all particles. The average height of small particles shown in Figure 7-b is different with that in Figure 7-a. Due to particle segregation and elutriation, the average height of small particles increases with time as

particles are uncharged or q_p is only 25% of the $|q|_{max}$. Nevertheless, the average height of small particles does not change anymore when the q_p increases to 50%, or even 100% of the $|q|_{max}$, which is attributed to the formation of agglomerates. When agglomerates are formed, small particles are attached to the big particles which avoid the particle segregation phenomenon of small particles. The average height of big particles is shown in Figure 7-c. In the simulations, the bed was packed by mostly big particles with a few small particles, therefore, the average height of big particles is almost the same with the average height of all particles as shown in Figure 7-a. Above all, electrostatic charges on particles has an effect on the height of the fluidized bed. In a certain range, electrostatic charges make the height of the fluidized bed increase, while extra charges accumulation leads to the formation of agglomerates and decreases the height of the fluidized bed.

4.3.2 Concentration distribution of small particles in the free board

Before analyzing the concentration distribution of small particles in the free board, it is necessary to determine the scope of the free board firstly. In general, the free board is the region above the surface of the fluidized bed, however in the turbulent regime, it is difficult to determine the free board inaccurately. Figure 8 gives the axial distributions of average solid concentration between 2 and 5 s in different cases. As shown in Figure 8, the average solid concentrations above 300 mm is lower than 0.04 at any charge level. Consequently, the area above 300 mm was taken to be representative of the free board in any case.

Figure 9 shows the axial distributions of average concentration of small particles between 2 and 5 s in the free board as particles carry different amount of charge. Figure 9 shows that the average concentration of small particles decreases as the height of the free board increases under the uncharged condition, which is consistent with the previous research [1]. For $q_p = 0.25|q|_{max}$, although the average concentration of small particles decreases along with the free board, the average concentration at any height between 300 and 500 mm is larger than the uncharged condition. The reason is thought to be that small particles are easy to be attached to big particles under electrostatic attractions and then they are sprayed out of the bed with big particles. But, these attached small particles will go back to the fluidized bed together with big particles eventually as they are transported in the free board, so average concentration of small particles in this case is lower than the uncharged case at any height above 500 mm. Moreover, as q_p reaches 50% or 100% of $|q|_{max}$, small particles only appear at a height range of

approximately 300 and 600 mm as a consequence of agglomerates, and some abnormal points at which the average concentration of small particles increases suddenly appear because of appearances of agglomerates. At these two larger levels of charge, small particles are splashed into the free board in the form of agglomerates. Because the terminal velocity of agglomerates is always larger than the superficial gas velocity, these small particles eventually fall back into the fluidized bed and are not elutriated. In other words, small particles only exist in the lower part of the free board and particle elutriation disappears. Besides of all, results in Figure 9 also proved the explanation in Section 4.1.2 that the deviation between the simulated elutriation rate and the empirical values is caused by the fact that the height of free space is lower than the transport disengagement height (TDH). When the height of free space is higher than the TDH, the average concentration of small particles will not decrease with the increasing height of free space and it will keep the same instead. In Figure 9, the average concentration of small particles still decreases with the increase of the height of free space when particles carry no charge. Therefore, the height of free space is lower than the transport disengagement height (TDH).

Figure 10 further displays the lateral distributions of average concentration of small particles between 2 and 5 s in the free board at different levels of charge. As shown in Figure 9, there almost exists no small particles in the upper part of the free board for $q_p = 0.5|q|_{max}$ or $|q|_{max}$. Therefore, Figure 10 only shows the cases in which particles are uncharged and q_p is 25% of the $|q|_{max}$. From Figure 10-a, as particles are uncharged, small particles at different heights of the free board all exhibit a core-annulus distribution, the small particles concentration near the wall is always larger than that in the core region. For q_p equals to 25% of $|q|_{max}$, core-annular solids lateral distribution of the small particles is still evident as shown in Figure 10. However, the solids concentration discrepancy between the core and annular region is reduced, which is revealed in Table 4. The electrostatic repulsive forces among positively charged small particles enhance the dispersion of small particle, further suppress the accumulation of small particle near the wall, and then make the solids discrepancy decrease. In the investigations of Pei et al. [47] and Wu et al. [48], they also found the formation of dispersed structures between similarly charged particles.

Table 4. Ranges and standard deviations of lateral concentration of small particles at different heights

Height (mm)	No charge		25% of the $\|q\|_{max}$	
	Range	Standard deviation	Range	Standard deviation
500-600	9.59×10^{-4}	3.41×10^{-4}	6.89×10^{-4}	2.48×10^{-4}
800-900	3.67×10^{-4}	1.36×10^{-4}	3.26×10^{-4}	9.47×10^{-5}
1100-1200	2.88×10^{-4}	1.02×10^{-4}	2.36×10^{-4}	6.76×10^{-5}

Overall, as particles are charged, the concentration distribution of small particles in the free board is changed. Compared to the case in which particles are uncharged, the concentration of small particles in the middle and upper part of the free board is reduced. Besides, although the lateral distribution form of small particles is not changed as particles are charged, but electrostatic repulsive forces reduce the lateral concentration differences of small particles in the middle and upper part of the free board.

4.3.3 Axial velocity distribution of small particles in the free board

The axial velocity of small particles in the free board is another important parameter which is used to investigate the mechanism of particle elutriation. Figure 11 shows the axial distribution of average axial velocity of small particles between 2 and 5 s in the free board at different levels of charge. Due to the rather low concentration of small particles in the free board at q_p of 50% or 100% of $|q|_{max}$, these two cases are not given in Figure 11. As shown in Figure 11, the average axial velocity of small particles increases along with the height of the free board under all the simulation condition. Comparing the average axial velocities of small particles at the same height between these two cases, the average axial velocity of small particles in the uncharged case is always larger at the height between 300 and 500 mm. Nevertheless, an opposite variation trend is observed above the height of 500 mm. In general, the elutriated small particles are transported in the free board with an initial velocity of the splashed velocity at the bed surface and their velocities vary along the freeboard all the time. As a consequence, the axial velocities of small particles in the free board are affected by both their splashed velocities and the accelerations. In the next section, these two factors are analyzed to reveal the differences of axial velocities between the two cases.

The splashed velocities of particles are related to the fluctuation intensity of the bed surface. The simulated standard deviations of average height with q_p equal to 25% of $|q|_{max}$ is 6.81 mm, while the standard deviations under uncharged condition is 11.81 mm. The simulated result is in consistent with the experimental results which is investigated by Dong et al. [16]. Weak fluctuations of the bed surface

lead to lower splashed velocities of particles, namely, lower initial velocities of particles. Therefore, in the lower part of the free board, the axial velocities of small particles in the charged case are lower.

Accelerations of particles are determined by forces acting on them. The gravity and drag force determine the motion of uncharged particles, while the charged particles bear more complex forces because of the electrostatic force. However, the effects of electrostatic forces on the particle acceleration is ignored in this research, because the electrostatic force (6.42×10^{-9}-2.47×10^{-8} N) in the axial direction was always lower than the resultant force of the gravity and the drag force (9.03×10^{-7}-3.41×10^{-6} N) by several orders of magnitude. Considering the fact that the drag force on a certain particle is the function of its slip velocity, its acceleration is determined by the difference between the gas velocity surrounding it and its own velocity. The axial distribution of average gas velocity between 2 and 5 s in the free board is shown in Figure 12. From Figure 12, the average gas velocities are almost the same at any height in these two cases, and they all equal to the superficial gas velocity approximately except in a small area near the bed surface where gas velocities are a little larger than the superficial gas velocity. Therefore, the accelerations of small particles are only determined by their own velocities in the free board and shows an reverse relation with their own velocities. So as the height of the free board increases, the increase of axial velocities of small particles results in the decrease of accelerations which results in the slowly increase of the small particle average axial velocity. Besides, the axial velocities of small particles in the uncharged case are larger than those under the charged condition especially for the lower part of the free board, so the axial velocities of small particles increase faster in the charged case because of greater acceleration. At a free board height of 500 mm, axial velocities of small particles become the same in different cases. However, Figure 10 illustrates that the lateral concentration differences of small particles between 500 and 600 mm were smaller since particles are charged. Considering the fact that the gas velocity is larger in the core region of the free board and lower near the wall at this height (showed in Figure 13), the increase of gas velocities around particles results in larger average accelerations for small particles in the charged case. So eventually, the average axial velocities of small particles in the charged case are larger than the uncharged case in the area above 500 mm.

In summary, electrostatic charges on particles affect the axial distribution of the axial velocity of small particles in the free board. As particles are charged, the reduction of fluctuation of the bed surface

results in lower splashed velocities of small particles. Moreover, the gas velocities around particles in the middle and upper part of the free board increases, because the particles are promoted from the wall area to the core region under the action of electrostatic repulsive forces. Furthermore, the accelerations of small particles increase, and electrostatic charges on particles make the axial velocities of small particles increase in the middle and upper part of the free board.

4.3.4 Particle agglomeration

In the preceding sections, agglomerations caused by electrostatic attractions have been raised several times. Essentially formation of agglomerates has an effect on the particle size distribution in the bed, so it is necessary to investigate the agglomerations and the particle size distribution under different charge levels. Figure 14 shows the instantaneous snapshots of the fluidized bed at 5 s for particles carrying various amounts of charge. As shown in Figure 14-a, uncharged particles are dispersed well in the bed. All particles separate at the bed surface and a distinct boundary can be observed. Besides, small particles show a core-annular distribution in upper part of the free board. As q_p reaches 25% of the $|q|_{max}$, the particles are still dispersed uniformly in the bed as shown in Figure 14-b. A close inspection, however, shows that some small particle are attached to big particles and the boundary between small particles and big particles becomes indistinct. Moreover, although small particles in the upper part of the free board also distribute in the form of core-annular distribution in this case, distances between particles become larger and the lateral concentration difference becomes smaller. Further increasing q_p to 50% of the $|q|_{max}$, Figure 14-c shows that there are no dispersed small particles in the fluidized bed, and the big particles are agglomerated by taking small particles as "bonder". By zooming in on the bed surface, agglomerates mainly exist in two forms, respectively, string and cluster. Figure 14-c also shows that at this level of charge, there are still few dispersed small particles in the free board. Eventually, as the charge reaches $|q|_{max}$, Figure 14-d shows that only agglomerates in the form of cluster can be observed in the bed.

Particle size distributions in the enlarged portions of the bed surface shown in Figure 14 are further calculated by pixel identification and shown in Figure 15. From this figure, uncharged particles exhibit a bimodal particle size distribution with two peaks at 1 and 0.5 mm, which correspond to the particle sizes of the big and small particles respectively. As particles are charged and q_p is 25% of the $|q|_{max}$, the particle size distribution is still bimodal with two peaks appearing at 1 and 0.5 mm, but the peak are

wider. Further increasing q_p to 50% of the $|q|_{max}$, two peaks change into a single wide peak. Finally, as the maximum amount of charge is approached, other new peaks appear around 4 mm and this translates to the appearance of agglomerates. Figure 15 further shows that agglomeration in the fluidized bed becomes more apparent and the agglomerates become larger, as electrostatic charges on particles increases.

4.3.5 Discussion

CFD-DEM results demonstrate that electrostatic charges on particles suppress the particle elutriation which is consistent with other investigations. Results in this work further show that electrostatic charges affect the hydrodynamic behavior of small particles in the fluidized bed and in the free board and consequently particle elutriation. Interestingly, not all effects suppress particle elutriation, some of them in fact promote particle elutriation. Firstly as shown in Section 4.3.1, electrostatic charges on particles increase the fluidized bed height. For a fluidized bed reactor, the height of the reactor is fixed, which means that the height of the free board is limited by the height of the fluidized bed. Therefore, the increase of the fluidized bed height decreases the height of the free board and increases the elutriation rate for a certain range. But, if the fluidized bed reactor is tall enough, and the height of the free board is larger than TDH, electrostatic effects on the height of the fluidized bed will not affect the elutriation rate. Secondly analysis in Section 4.3.2 reveals that electrostatic charges on particles increase the concentration of small particle in the lower part of the free board, while parts of small particles in this area attach themselves onto big particles and fall back into the fluidized bed. Eventually concentration of small particles in the upper part of the bed decrease and elutriation of fine particles is suppressed. In section 4.3.3, electrostatic charges on particles decrease the splashed velocities of small particles since the fluctuation of the bed surface decreases. But as small particles reach the upper part of the free board, parts of particles move from the region near the wall to the core region of the reactor under electrostatic repulsive forces. The axial velocities of small particles in the upper part of the free board increase and the elutriation is promoted. However, from the modeling results, particle elutriation is suppressed by electrostatic forces. So it can be concluded that the effect of attachment between small particles and big particles caused by electrostatic attractions, namely the agglomeration, is always the most important factor which dominates the electrostatic effects.

According to the conclusion raised above, as one uses a correlation developed by experiments which has eliminated electrostatic effects to predict the elutriation rate in an industrial system, electrostatic effects must be considered by using an electrostatic coefficient χ_e (χ_e＜1). This coefficient is the function of the amount of charge on particles and in theory it can be acquired by experiments. Nevertheless, it is a pity that there are currently no experimental methods to control the amount of charge on particles precisely and quantitatively, so the CFD-DEM modeling used in this work may be the best way to acquire this coefficient. Previous investigations have raised an idea about controlling particle elutriation by using electrostatic forces [49]. Results in this work supply a possibility for this idea, but the amount of charge on particles should be controlled in a proper range. In this work, 25% of the $|q|_{max}$ might be the proper one. Just shown in Figure 6, as q_p was 25% of the $|q|_{max}$, particle elutriation is suppressed, but as shown in Figure 14-b, particles in the bed are still dispersed well, and no large agglomerates are observed.

5. Conclusion

Due to the drawbacks of existing methods, the electrostatic effects on particle elutriation is still unclear. This work for the first time uses the CFD-DEM modeling approach to investigate particle elutriation taking into account electrostatic effects on particle elutriation. These following conclusions can be drawn from this study:

(1) CFD-DEM modeling is suitable for investigating particle elutriation. The predicted elutriation rate increases with increasing superficial gas velocity and which is in good agreement with the results computed from an empirical correlation developed for an experimental system similar to the present work.

(2) The CFD-DEM predictions show that at the same superficial gas velocity, as amount of charge on particles increases, the elutriation rate decreases. The results also show that in theory, particle elutriation might disappear as the amount of charge on particles increases to significantly high values.

(3) The fundamental mechanism of static electricity on particle elutriation is a kind of multifactor effect mechanism in which agglomeration caused by electrostatic attractions is the most dominant. Electrostatic charges on particles may result in the increase of the fluidized bed height, the axial velocity of small particles in the upper part of the free board and then promoted particle elutriation. But meanwhile, charges on particles will lead to agglomeration, decrease the concentration of small

particles in the upper part of the free board and then suppressed particle elutriation.

In summary, static electricity in fluidized beds has multifactor effects on particle elutriation. When the electrostatic effects on particle elutriation are studied by experiments, it is necessary to focus on the hydrodynamic behaviors in the fluidized bed, the dynamic behaviors of small particles in the free boards and especially the agglomerates caused by electrostatic attractions. In addition, it is worth mentioning that limited by computational capability, only a thin bed was used in this paper, so although simulated results in this paper have shown that CFD-DEM simulation can be used to investigate the particle elutriation, it is unavoidable that the results have been influenced by the extra frictions between particles and the front/back wall. Therefore, in order to give a more comprehensive understanding of the particle elutriation and engineering application, it is necessary to investigate it in a three-dimension or pseudo-three-dimensional fluidized bed in the future.

Acknowledgements

The authors acknowledge the support and encouragement of the National Natural Science Foundation of China (Grant 21236007), The National Science Fund for Distinguished Young (Grant 21525627), Specialized Research Fund for the Doctoral Program of Higher Education (Grant 20130101110063) and the natural science foundation of Zhejiang province (Grant No. LR14B060001).

Nomenclature

A	cross-sectional area of the fluidized bed, m^2
C_D	drag coefficient, dimensionless
d_p	particle diameter, m
$E_{i\infty}$	elutriation rate, $kg/m^2 \cdot s$
$\mathbf{f_c}$	contact force, N
$\mathbf{f_d}$	drag force, N
$\mathbf{f_e}$	inter-particle electrostatic force, N
$\mathbf{f_p}$	far field pressure force, N
$\mathbf{g}$	gravitational acceleration, m/s^2
$<h_p>$	average height of particles, m
I	particle moment of inertia, $kg \cdot m^2$
k	turbulent kinetic energy, m^2/s^2

k_n	spring coefficient in normal direction, N/m
k_t	spring coefficient in tangential direction, N/m
K	elutriation rate constant, s^{-1}
K_B	Boltzmann's constant, J/K
m	particle mass, kg
$\mathbf{M_r}$	rolling resistant torque, N·m
$\mathbf{M_t}$	torque in tangential direction, N·m
N	number of particle for statistic
P	pressure, Pa
q	particle charge, C
$\mathbf{r_i}$	radius vector from particle center to contact point, m
$\mathbf{S}_{s\rightarrow g}$	fluid-particle interaction source, N/m^3
T	temperature, K
u_0	superficial gas velocity, m/s
u_c	transition velocity, m/s
u_t	terminal velocity of particles, m/s
$\mathbf{u}$	gas velocity, m/s
$\mathbf{v}$	particle velocity, m/s
V	particle volume, m^3
V_c	volume of the present computational cell, m^3
W	total mass of the specific particles, kg
X_i	mass fraction of particle *i*, dimensionless

Greek symbols

β	inter-phase momentum transfer coefficient, $kg/m^3 \cdot s$
ε_o	relative permittivity of free board, F/m
ε_g	volume fraction, dimensionless
ε_r	relative permittivity of particles, dimensionless
ε_s	solid fraction, dimensionless
ε_t	turbulent dissipation rate, m^2/s^3

η_n	damping coefficients in normal direction, kg/s
η_t	damping coefficients in tangential direction, kg/s
κ	inverse of the Debye length, m^{-1}
μ_f	dynamic friction coefficient, dimensionless
μ_g	gas viscosity, kg/m·s
μ_r	rolling resistance coefficient, dimensionless
ρ_g	gas density, kg/m^3
ρ_p	particle density, kg/m^3
σ_{nij}	normal displacements between particle *i* and particle *j*, m
σ_{tij}	tangential displacements between particle *i* and particle *j*, m
χ_e	electrostatic coefficient, dimensionless
$\boldsymbol{\omega}$	rotational velocity, 1/s

Subscripts

g	gas
n	normal direction
p	particle
s	solid
t	tangential direction

References

[1] M. Kwauk, H. Li, Handbook of fluidization, Beijing: Chemical Industry Press, 2007.

[2] T.A. Alsmari, J.R. Grace, X.T. Bi, Effects of superficial gas velocity and temperature on entrainment and electrostatics in gas-solid fluidized beds, Chemical Engineering Science, 123 (2015) 49-56.

[3] J.W. Chew, A. Cahyadi, C.M. Hrenya, R. Karri, R.A. Cocco, Review of entrainment correlations in gas-solid fluidization, Chemical Engineering Journal, 260 (2015) 152-171.

[4] W. Nicol, E. du Toit, W. de Vos, Dynamic elutriation measurement in a continuously operated bubbling fluidized bed, The 13th International Conference on Fluidization-New Paradigm in Fluidization Engineering, bepress, 2011, pp. 22.

[5] S. Yagi, T. Aochin, Paper presented at the Spring Meeting of the Society of Chemical Engineers, Japan, (1955).

[6] D. Santana, J. Rodrıguez, A. Macıas-Machın, Modelling fluidized bed elutriation of fine particles, Powder technology, 106 (1999) 110-118.

[7] J. Choi, I. Chang, D. Shun, C. Yi, J. Son, S. Kim, Correlation on the particle entrainment rate in gas fluidized beds, Industrial & engineering chemistry research, 38 (1999) 2491-2496.

[8] J. Choi, J. Suh, I. Chang, D. Shun, C. Yi, J. Son, S. Kim, The effect of fine particles on elutriation of coarse particles in a gas fluidized bed, Powder technology, 121 (2001) 190-194.

[9] I. Tanaka, H. Shinohara, H. Hirosue, Y. Tanaka, Elutriation of fines from fluidized bed, Journal of Chemical Engineering of Japan, 5 (1972) 51-57.

[10] C. Wen, L. Chen, Fluidized bed freeboard phenomena: entrainment and elutriation, AIChE Journal, 28 (1982) 117-128.

[11] F. Milioli, P. Foster, Entrainment and elutriation modelling in bubbling fluidized beds, Powder technology, 83 (1995) 233-244.

[12] D. Geldart, The effect of fines on entrainment from gas fluidized beds, Trans. Inst. Chem. Eng., 57 (1979) 269-275.

[13] J. Cross, Electrostatics: principles, problems and applications, (1987).

[14] P. Jiang, H. Bi, S.C. Liang, L.S. Fan, Hydrodynamic behavior of circulating fluidized bed with polymeric particles, AIChE journal, 40 (1994) 193-206.

[15] L. Jiang, X. FangZhi, L. ZhengHong, A CFD modeling of the gas-solid two-phase flow in an FCC riser under the electrostatic conditions, Asia‐Pacific Journal of Chemical Engineering, 9 (2014) 645-655.

[16] K. Dong, Q. Zhang, Z. Huang, Z. Liao, J. Wang, Y. Yang, Experimental investigation of electrostatic effect on bubble behaviors in gas-solid fluidized bed, AIChE Journal, (2015).

[17] S. Tasirin, D. Geldart, Entrainment of FCC from fluidized beds — A new correlation for the elutriation rate constants $K_{i\infty}^*$, Powder Technology, 95 (1998) 240-247.

[18] T. Baron, C.L. Briens, M.A. Bergougnou, J.D. Hazlett, Electrostatic effects on entrainment from a fluidized bed, Powder Technology, 53 (1987) 55-67.

[19] C.L. Briens, M.A. Bergougnou, I.I. Inculet, T. Baron, J.D. Hazlett, Size distribution of particles entrained from fluidized beds: Electrostatic effects, Powder Technology, 70 (1992) 57-62.

[20] J. Li, K. Kato, Effect of electrostatic and capillary forces on the elutriation of fine particles from a fluidized bed, Advanced Powder Technology, 12 (2001) 187-205.

[21] X. Ma, K. Kato, Effect of interparticle adhesion forces on elutriation of fine powders from a fluidized bed of a binary particle mixture, Powder Technology, 95 (1998) 93-101.

[22] S. Nieh, G. Yang, A. Zhu, C. Zhao, Measurements of gas-particle flows and elutriation of an 18 inch id cold vortexing fluidized-bed combustion model, Powder technology, 69 (1992) 139-146.
[23] H. Hatano, M. Ishida, Study on the entrainment of FCC particles from a fluidized bed, Powder Technology, 35 (1983) 201-209.
[24] X.-Z. Chen, D.-P. Shi, X. Gao, Z.-H. Luo, A fundamental CFD study of the gas–solid flow field in fluidized bed polymerization reactors, Powder Technology, 205 (2011) 276-288.
[25] L. Jiang, X. Fang‐Zhi, L. Zheng‐Hong, A CFD modeling of the gas–solid two‐phase flow in an FCC riser under the electrostatic conditions, Asia‐Pacific Journal of Chemical Engineering, 9 (2014) 645-655.
[26] G. Chen, Q. Su, Z. Luo, Modeling the electrostatic effect on the hydrodynamic behavior in FCC risers: From understanding to application, Particuology, 25 (2016) 122-132.
[27] H. Pan, X.-Z. Chen, X.-F. Liang, L.-T. Zhu, Z.-H. Luo, CFD simulations of gas–liquid–solid flow in fluidized bed reactors — A review, Powder Technology, 299 (2016) 235-258.
[28] R.G. Rokkam, R.O. Fox, M.E. Muhle, Computational fluid dynamics and electrostatic modeling of polymerization fluidized-bed reactors, Powder Technology, 203 (2010) 109-124.
[29] N. Deen, M.V.S. Annaland, M. Van der Hoef, J. Kuipers, Review of discrete particle modeling of fluidized beds, Chemical Engineering Science, 62 (2007) 28-44.
[30] E.W.C. Lim, Y. Zhang, C. Wang, Effects of an electrostatic field in pneumatic conveying of granular materials through inclined and vertical pipes, Chemical Engineering Science, 61 (2006) 7889-7908.
[31] S. Yang, K. Luo, M. Fang, K. Zhang, J. Fan, Parallel CFD-DEM modeling of the hydrodynamics in a lab-scale double slot-rectangular spouted bed with a partition plate, Chemical Engineering Journal, 236 (2014) 158-170.
[32] Z. Zhou, S. Kuang, K. Chu, A. Yu, Discrete particle simulation of particle-fluid flow: model formulations and their applicability, Journal of Fluid Mechanics, 661 (2010) 482-510.
[33] E.W.C. Lim, Mixing behaviors of granular materials in gas fluidized beds with electrostatic effects, Industrial & Engineering Chemistry Research, 52 (2013) 15863-15873.
[34] M.A. Hassani, R. Zarghami, H.R. Norouzi, N. Mostoufi, Numerical investigation of effect of electrostatic forces on the hydrodynamics of gas-solid fluidized beds, Powder Technology, 246 (2013) 16-25.
[35] M.D. Hogue, C.I. Calle, P.S. Weitzman, D.R. Curry, Calculating the trajectories of triboelectrically charged particles using Discrete Element Modeling (DEM), Journal of Electrostatics, 66 (2008) 32-38.
[36] B.E. Launder, D. Spalding, The numerical computation of turbulent flows, Computer methods in applied mechanics and engineering, 3 (1974) 269-289.
[37] S. Kuang, A. Yu, Z. Zou, Computational study of flow regimes in vertical pneumatic conveying, Industrial & Engineering Chemistry Research, 48 (2009) 6846-6858.
[38] S. Matsusaka, H. Maruyama, T. Matsuyama, M. Ghadiri, Triboelectric charging of powders: A review, Chemical Engineering Science, 65 (2010) 5781-5807.
[39] C. Pei, C. Wu, D. England, S. Byard, H. Berchtold, M. Adams, Numerical analysis of contact electrification using DEM–CFD, Powder Technology, 248 (2013) 34-43.
[40] C. Pei, C. Wu, M. Adams, D. England, S. Byard, H. Berchtold, Contact electrification and charge distribution on elongated particles in a vibrating container, Chemical Engineering Science, (2014).
[41] W. Fang, W. Jingdai, Y. Yongrong, Distribution of electrostatic potential in a gas-solid fluidized bed and measurement of bed level, Industrial & Engineering Chemistry Research, 47 (2008) 9517-9526.
[42] M. Horio, Circulating fluidized bed technology Ⅲ, Pergamon1991.

[43] H.T. Bi, Flow regime transitions in gas-solid fluidization and transport [D], Vancouver: University of British Columbia, 1994.

[44] J.R. van Ommen, S. Sasic, J. van der Schaaf, S. Gheorghiu, F. Johnsson, M.O. Coppens, Time-series analysis of pressure fluctuations in gas-solid fluidized beds—A review, International Journal of Multiphase Flow, 37 (2011) 403-428.

[45] Y. Feng, A. Yu, Effect of bed thickness on the segregation behavior of particle mixtures in a gas fluidized bed, Industrial & Engineering Chemistry Research, 49 (2010) 3459-3468.

[46] M. Goldschmidt, R. Beetstra, J. Kuipers, Hydrodynamic modelling of dense gas-fluidised beds: comparison and validation of 3D discrete particle and continuum models, Powder Technology, 142 (2004) 23-47.

[47] C. Pei, C. Wu, D. England, S. Byard, H. Berchtold, M. Adams, DEM-CFD modelling of particle systems with long-range electrostatic interactions, AIChE Journal, 61 (2015) 1792-1803.

[48] S. Wu, D. Wasan, A. Nikolov, Two-dimensional self-assembly of similarly charged granular particles, Industrial & Engineering Chemistry Research, 47 (2007) 5005-5015.

[49] G. Hendrickson, Electrostatics and gas phase fluidized bed polymerization reactor wall sheeting, Chemical Engineering Science, 61 (2006) 1041-1064.

Figure list

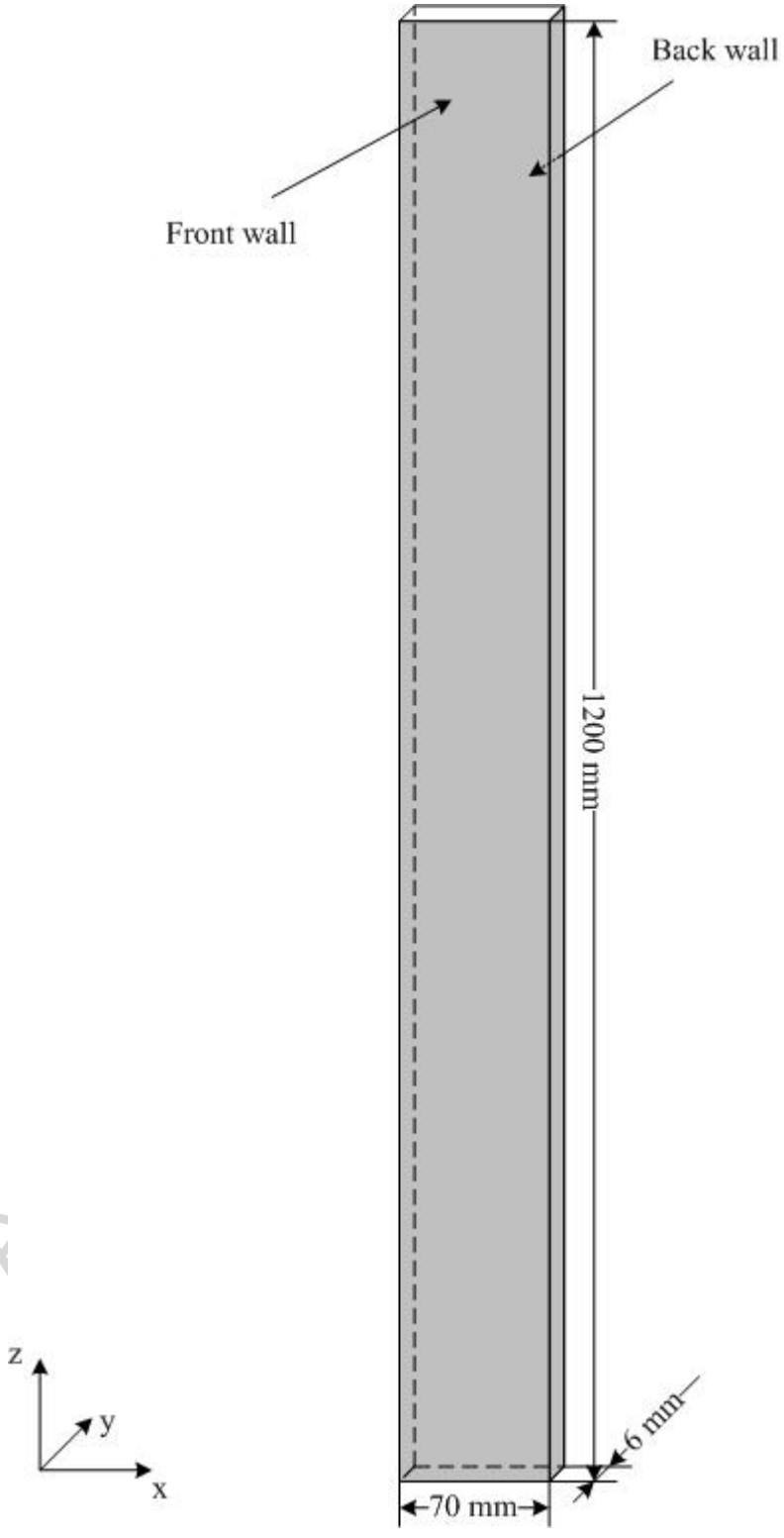

Fig. 1

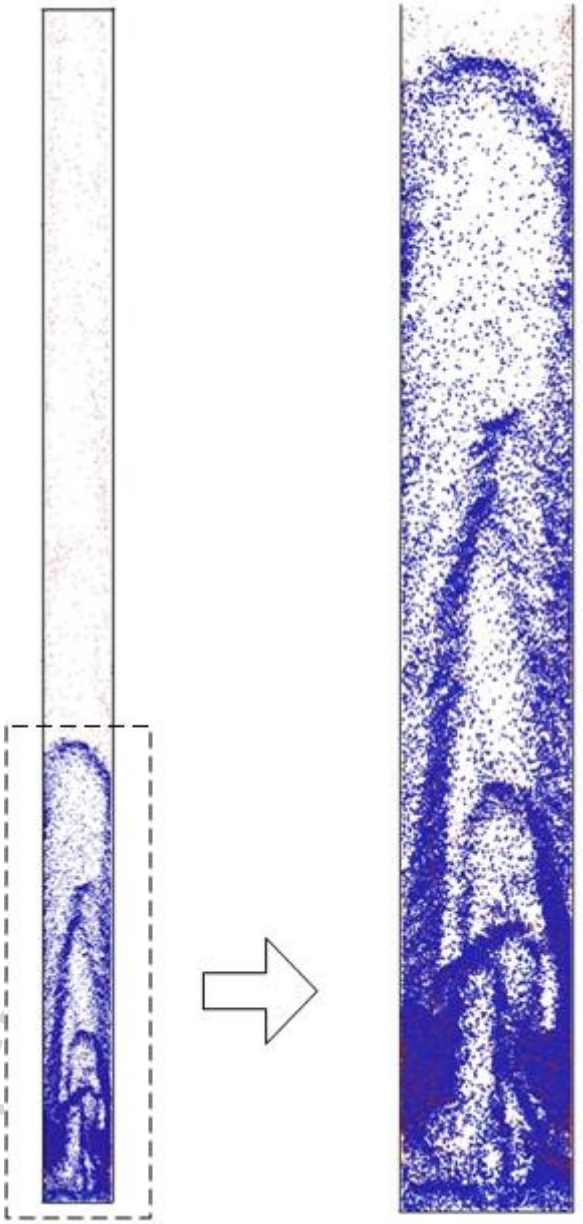

Fig. 2

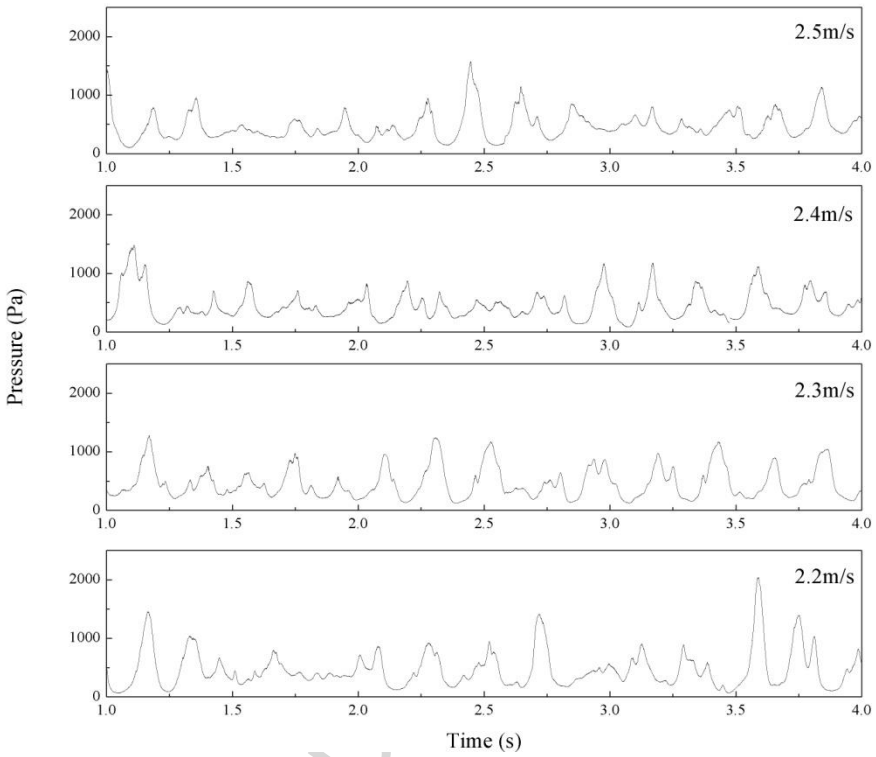

Fig. 3

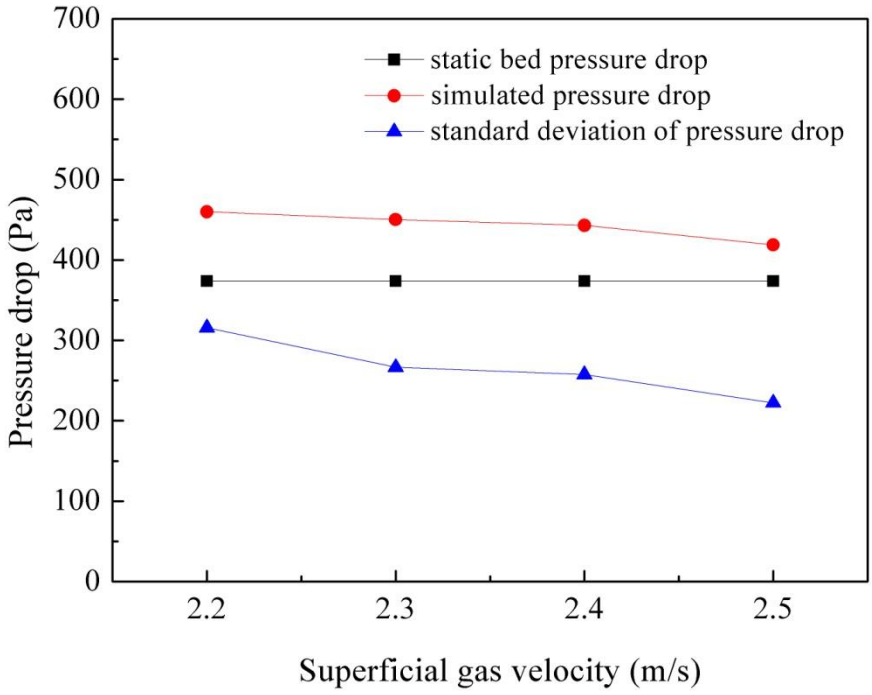

Fig. 4

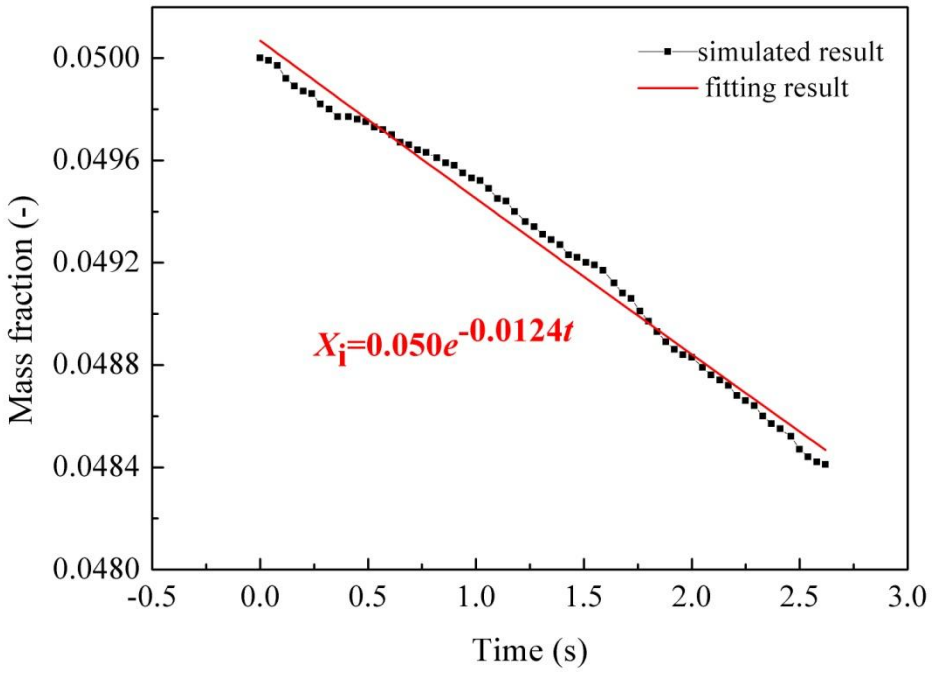

Fig. 5

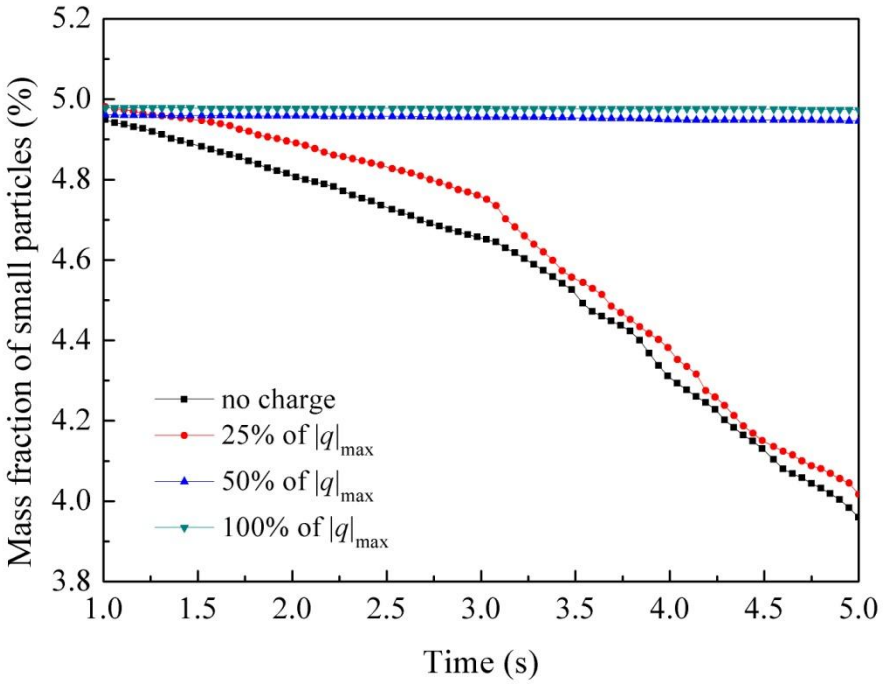

Fig. 6

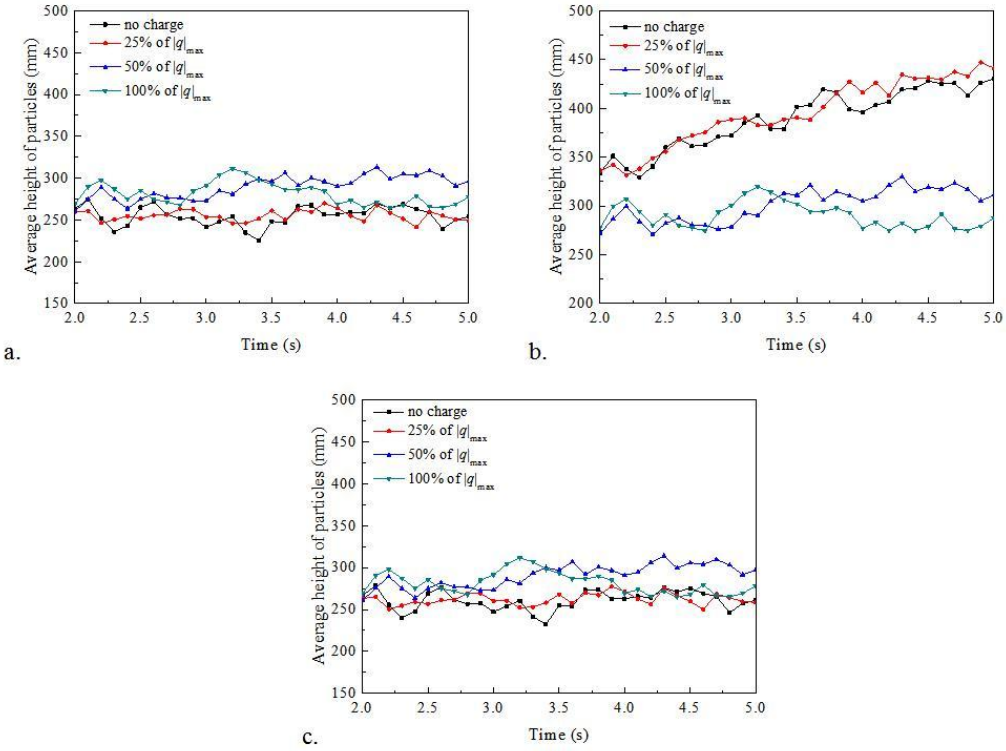

Fig. 7

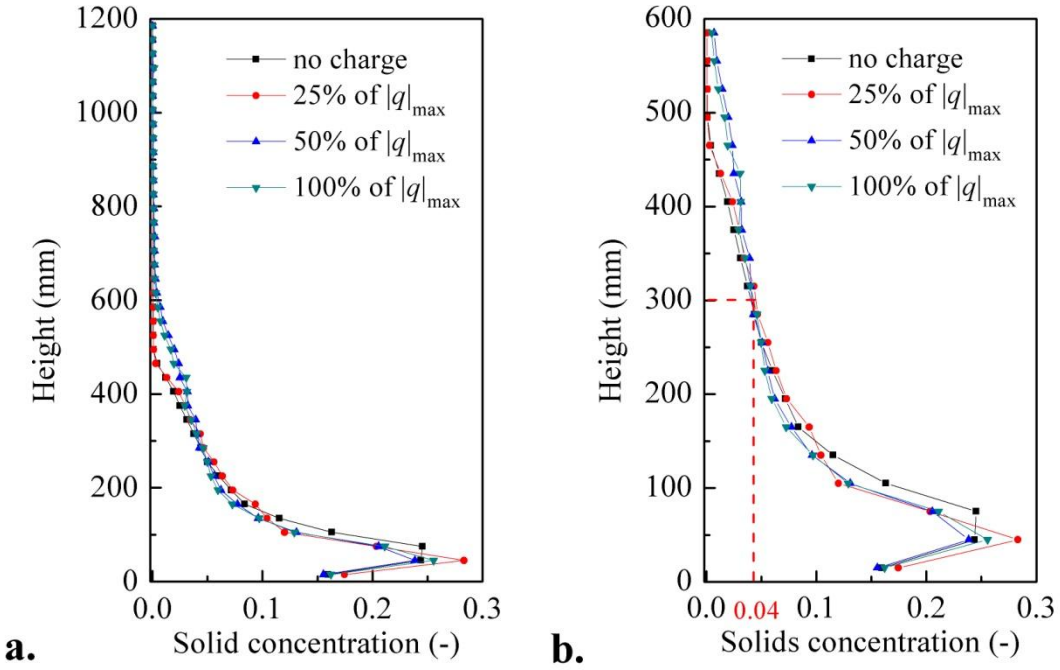

Fig. 8

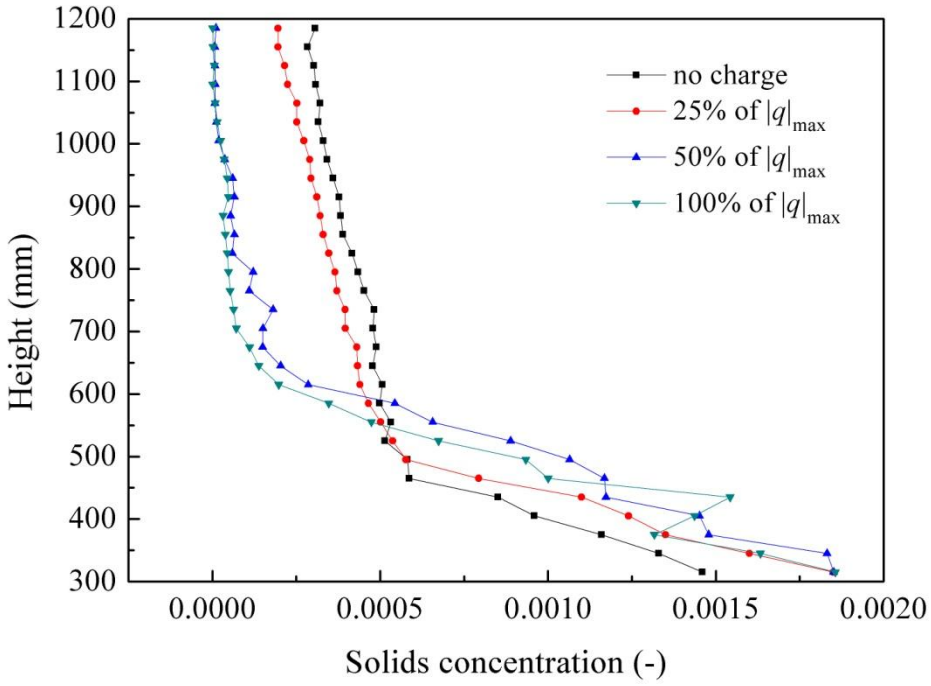

Fig. 9

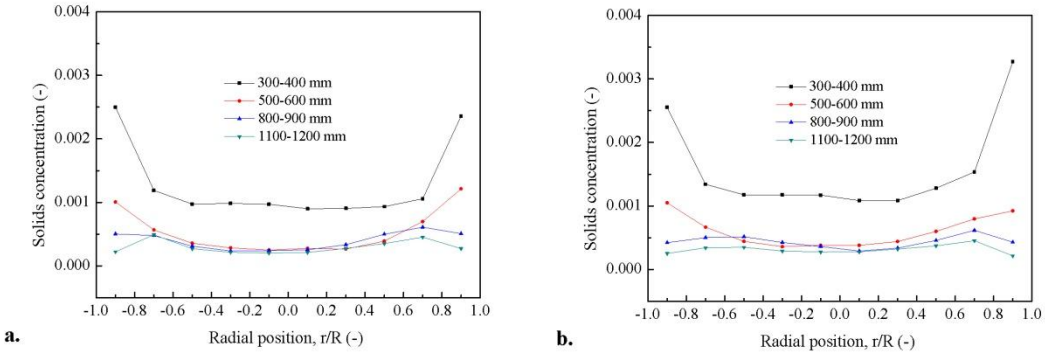

Fig. 10

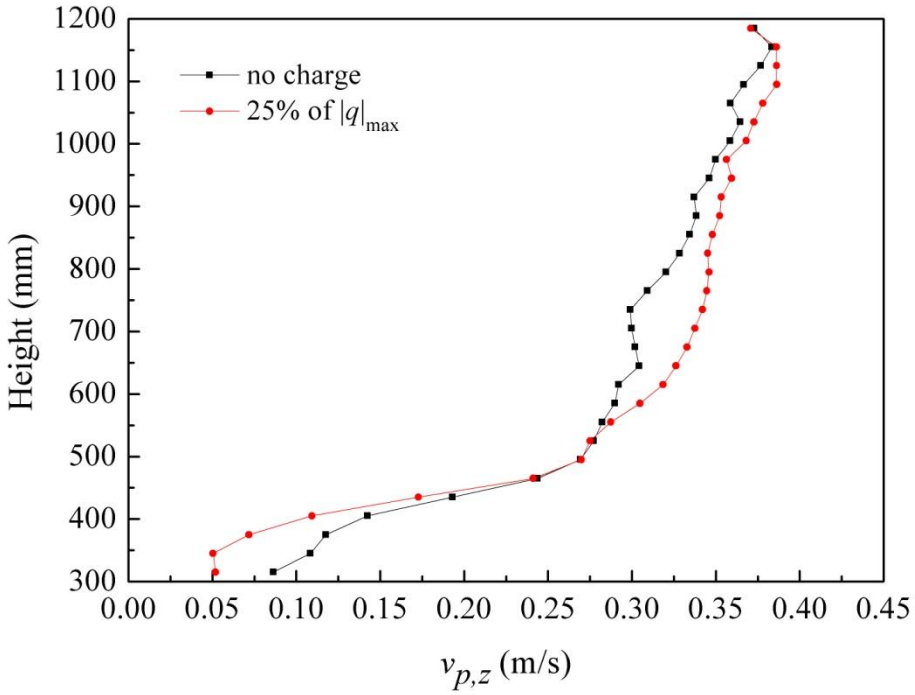

Fig. 11

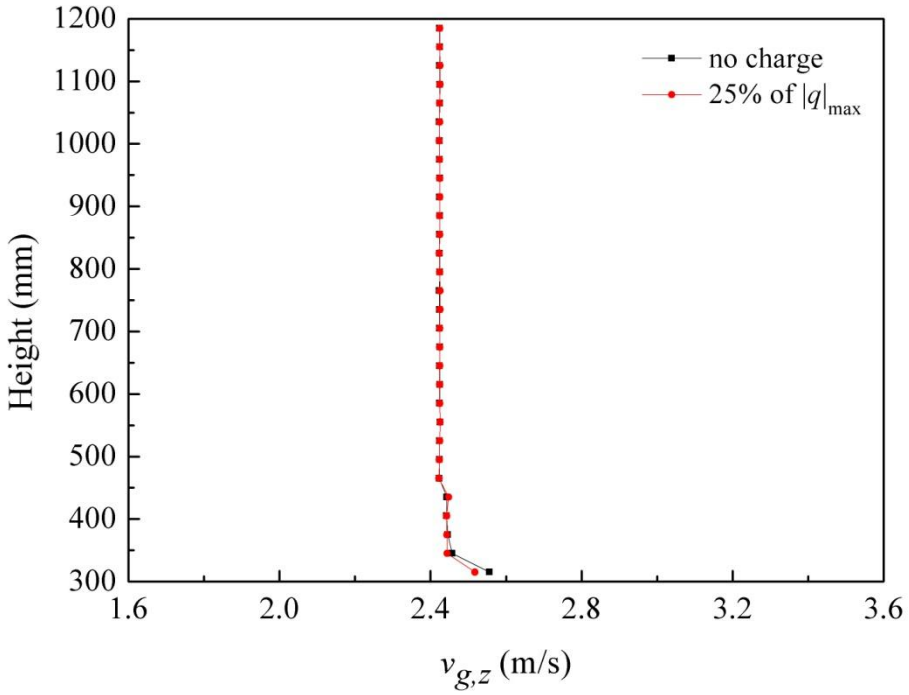

Fig. 12

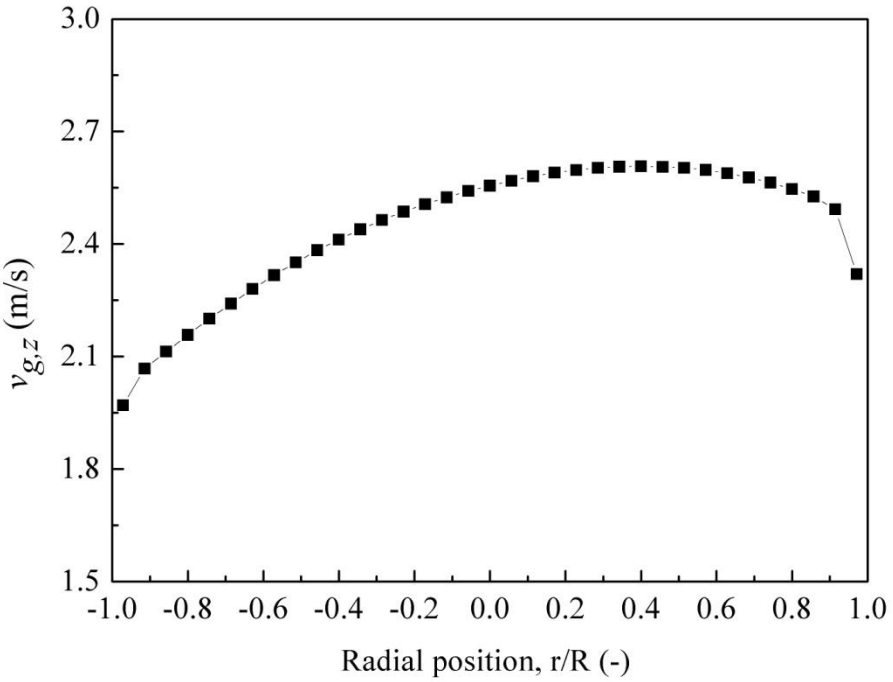

Fig. 13

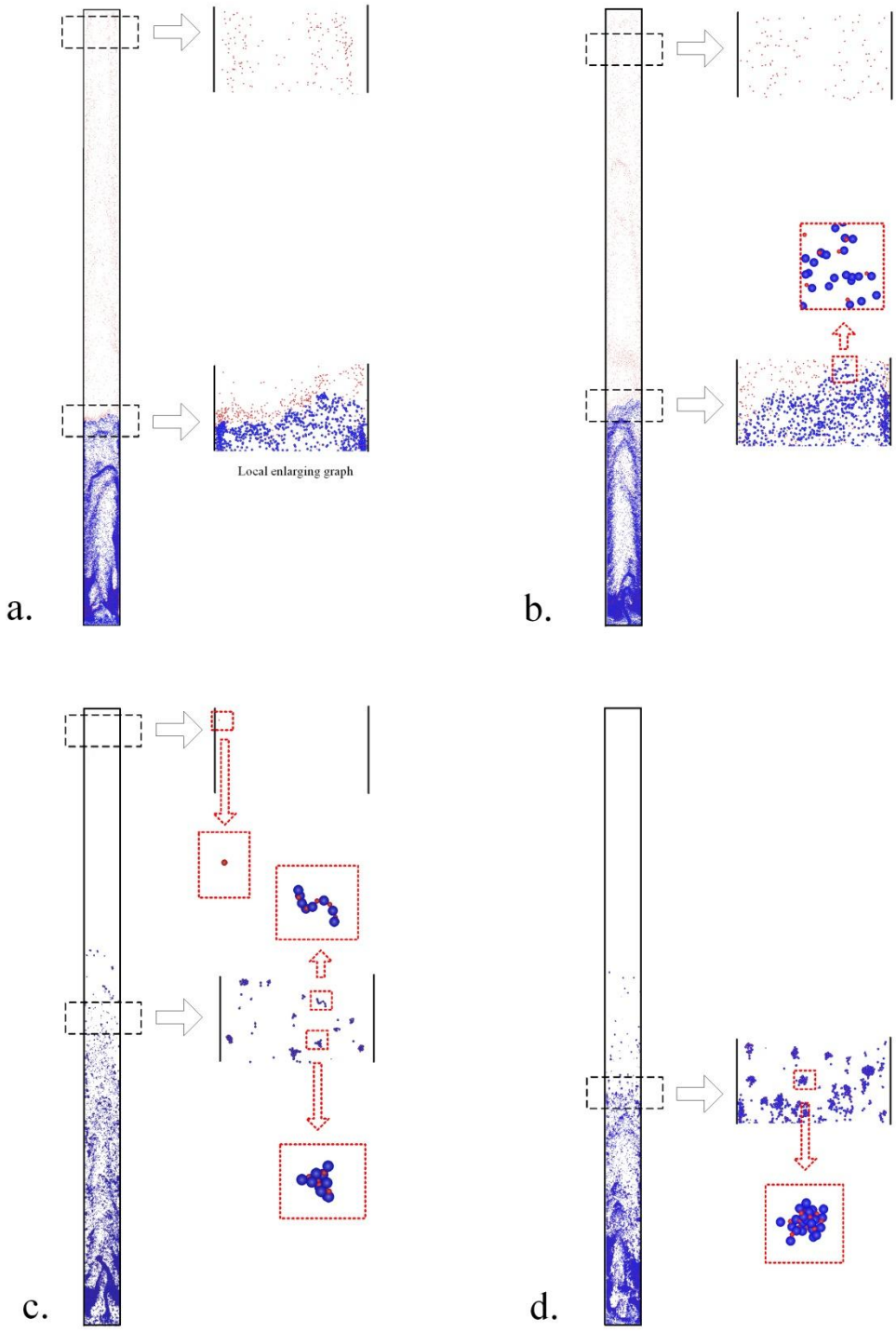

Fig. 14

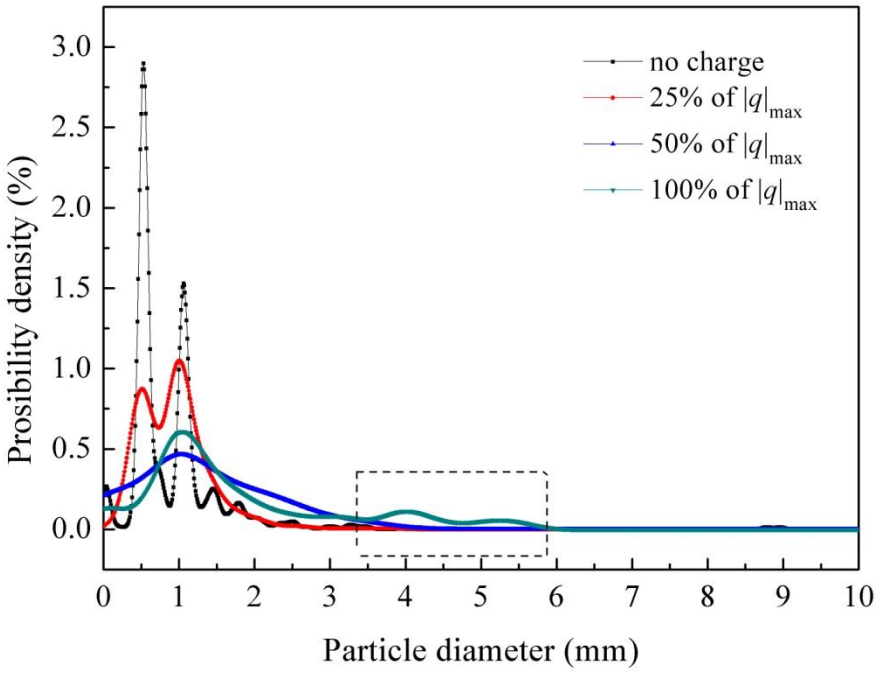

Fig. 15

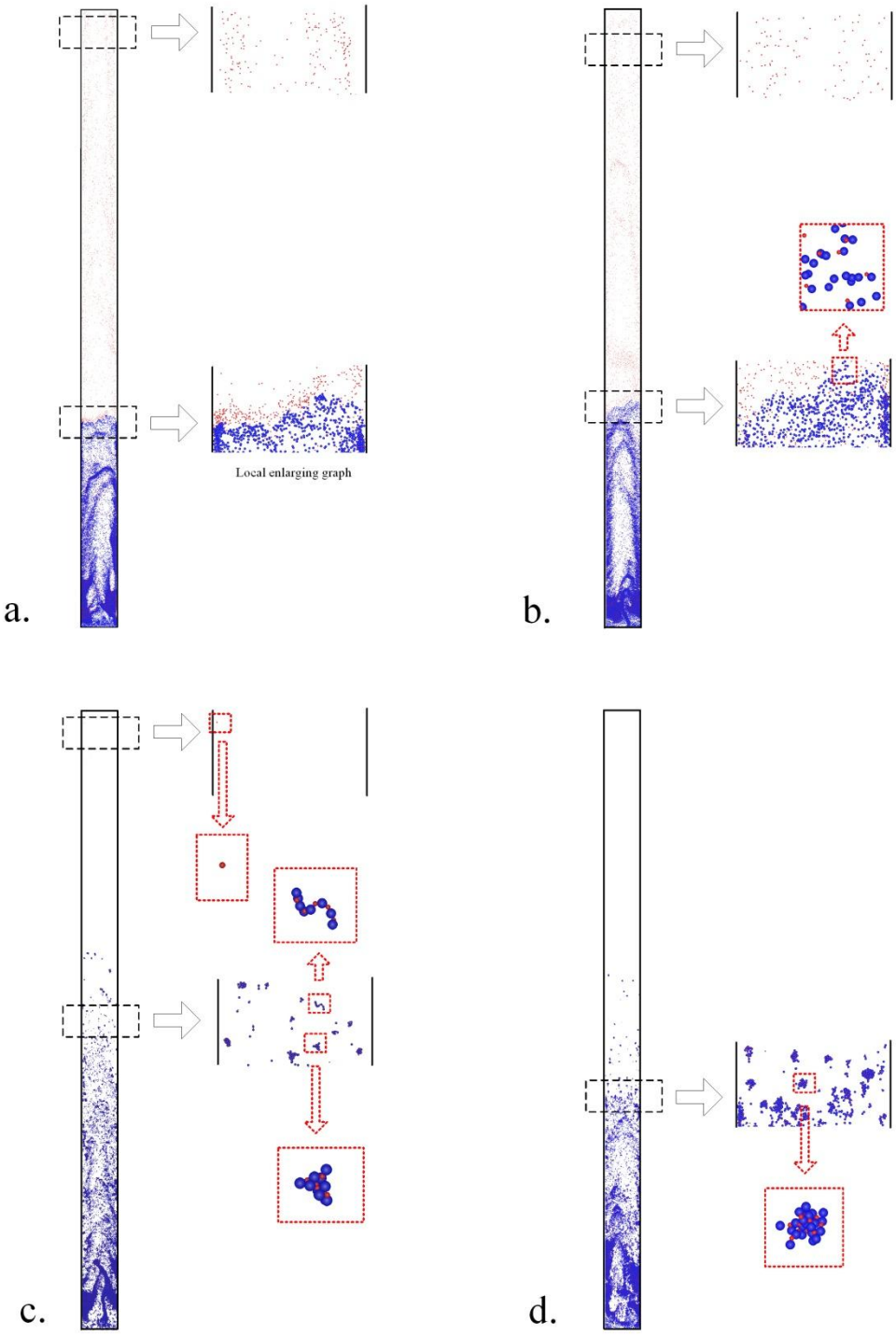

Graphical abstract

Highlights

1. Particle elutriation is for the first time studied by CFD-DEM modeling

2. Electrostatic effects on particle elutriation is studied by CFD-DEM modeling

3. Simulated results showed that static electricity suppressed particle elutriation

4. Effect mechanism of static electricity is a kind of multifactor effect mechanism

5. In the multifactor effect mechanism, agglomerates is the most predominant